Soft computing approach for prediction of surface settlement induced by earth pressure balance shield tunneling

W.G. Zhang [a,b,c], H.R. Li [c], C.Z. Wu [c], Y.Q. Li [c], Z.Q. Liu [d], H.L. Liu [a,b,c,*]

[a] *Key Laboratory of New Technology for Construction of Cities in Mountain Area, Chongqing University, Chongqing 400045, China*
[b] *National Joint Engineering Research Center of Geohazards Prevention in the Reservoir Areas, Chongqing University, Chongqing 400045, China*
[c] *School of Civil Engineering, Chongqing University, Chongqing 400045, China*
[d] *Norwegian Geotechnical Institute (NGI), Sognsveien 72, 0855 Oslo, Norway*

Abstract

Estimating surface settlement induced by excavation construction is an indispensable task in tunneling, particularly for earth pressure balance (EPB) shield machines. In this study, predictive models for assessing surface settlement caused by EPB tunneling were established based on extreme gradient boosting (XGBoost), artificial neural network, support vector machine, and multivariate adaptive regression spline. Datasets from three tunnel construction projects in Singapore were used, with main input parameters of cover depth, advance rate, earth pressure, mean standard penetration test (SPT) value above crown level, mean tunnel SPT value, mean moisture content, mean soil elastic modulus, and grout pressure. The performances of these soft computing models were evaluated by comparing predicted deformation with measured values. Results demonstrate the acceptable accuracy of the model in predicting ground settlement, while XGBoost demonstrates a slightly higher accuracy. In addition, the ensemble method of XGBoost is more computationally efficient and can be used as a reliable alternative in solving multivariate nonlinear geo-engineering problems.

Keywords: EPB; Surface settlement; Soft computing; XGBoost; Multivariate adaptive regression spline

1 Introduction

Recently, land has been utilized more, both above and below ground, and urban underground space has been developed rapidly, such as the construction of urban subway networks and underground shopping malls. A key issue that must be addressed is the effect of tunneling on the deformation of adjacent soil. If the deformation exceeds a critical value, economic losses to a project may be incurred (Bilgin, Ozbayir, Sozak, & Eyigun, 2009). To reduce ground settlement caused by soil release stress and avoid this situation as much as possible, an earth pressure balanced shield is frequently used in soft soil, which utilizes mud pressure to balance the tunnel front face pressure to minimize the effect on the surrounding deformation, particularly in urban environments comprising dense buildings (Bouayad, Emeriault, & Maza, 2015). However, even with this tunneling method, it is still challenging to determine the surface settlement.

Experts have used various theories to calculate surface deformation, which can be divided into theoretical calculations, experimental and numerical simulations, and machine learning methods. As theoretical calculations are typically more complicated, which involve many parameters, a few factors can be ignored for simplifying the calculation to establish an empirical formula (Mair, Taylor, & Bracegirdle, 1993; Loganathan & Poulos, 1998; Verruijt & Booker, 1996; Chou & Bobet, 2002; Park, 2005). Although solving problems experimentally is feasible, it is

---

* Corresponding author at: Key Laboratory of New Technology for Construction of Cities in Mountain Area, Chongqing University, Chongqing 400045, China.
 E-mail address: hliuhhu@163.com (H.L. Liu).

time consuming and the cost incurred is high (Chapman, Ahn, & Hunt, 2007; Marshall, Farrell, Klar, & Mair, 2012; Fang, Chen, Tao, Cui, & Yan, 2019; Lu, Shi, Wang, & Wang, 2019). Models used in numerical simulations are visually strong and intuitive. Researchers have established several models to predict tunneling-induced deformation for different projects (Mroueh & Shahrour, 2002; Ng & Lee, 2005; Ocak, 2009; Ercelebi, Copur, & Ocak, 2011; Chakeri, Hasanpour, Hindistan, & Ünver, 2011; Lambrughi, Rodríguez, & Castellanza, 2012; Gong et al., 2014; Huang et al., 2015; Huang, Huang, Ye, Zhang, & Zhang, 2018; Xiang et al., 2018; Chen, Wang, & Zhang, 2019). However, owing to software setting, a few parameters that must be assigned in the modeling process are neglected. Moreover, the constitutive model of soil is generally assumed and cannot reflect the actual stratum properties well when the stratum changes in a complex manner. An inevitable error will occur between the calculated and actual values.

To avoid an artificially assumed interference, machine learning is highly recommended for mapping all input variables to the response. The principle of this method is equivalent to an expert learning a significant amount of data to understand the relationship between the result and characteristic variables. Hence, a new case can be assessed and prediction results can be obtained. This process does not disregard any information and maximizes the utilization of the dataset obtained. Hence, many different machine learning methods have been applied to study such geotechnical problems (Kim et al., 2001; Neaupane & Adhikari, 2006; Suwansawat & Einstein, 2006; Santos & Celestino, 2008; Cheng, Tsai, Ko, & Chang, 2008; Yao, Yang, Yao, & Sun, 2010; Xu & Xu, 2011; Adoko, Zuo, & Wu, 2011; Mahdevari & Torabi, 2012; Mahdevari, Torabi, & Monjezi, 2012; Wang, Qiu, Xie, & Wang, 2012; Ahangari, Moeinossadat, & Behnia, 2015; Kohestani & Bazarganlari, 2017; Ding, Wei, & Wei, 2017; Goh, Zhang, Zhang, Xiao, & Xiang, 2018; Zhang, Wu, Li, Wang, & Samui, 2021; Zhang, Zhang, Wu, et al., 2020). Adoko et al. (2013) established the predicting model of the diameter convergence of a high-speed railway tunnel in weak rock based on multivariate adaptive regression spline (MARS) and artificial neural network (ANN). Ocak and Seker (2013) used three different methods: ANN, support vector machine (SVM), and Gaussian processes (GPs) to predict the surface settlement of Istanbul Metro tunnels excavated by earth pressure balance-tunnel boring machine (EPB-TBM). In addition, the partial least-squares regression models were adapted to link ground surface displacements to TBM operation parameters for two groups of observations during the construction of the Toulouse (France) subway line B tunnel (Bouayad et al., 2015). Furthermore, the characteristic parameter analysis of mix shield tunneling was presented using K-means clustering and meaningful protection measures for the Nanning metro line were discussed (Xie, Wang, Huang, & Qi, 2018).

However, the application methods above are mostly single sophisticated algorithms. Nanni and Lumini (2009) and Lessmann, Baesens, Seow, and Thomas (2015) reported that ensemble methods are better than single machine learning and other statistical methods, as they improve machine learning speed and results reliability by combining multiple models and therefore produce better predictions.

Therefore, this paper proposes development models that combine ensemble learning extreme gradient boosting (XGBoost) and three classical machine learning methods, including ANN, SVM, and MARS to predict the maximum settlement caused by EPB tunneling projects in Singapore. A brief introduction of these four methods is presented in the following section. In addition, a case study is provided, which primarily introduces the geological conditions and data collection related to the projects. The fourth section explains the prediction performances of four models and provides comparison analyses in detail. Meanwhile, feature importance analyses are presented in the discussion section. The main conclusions are summarized in the final section.

2 Methodology

2.1 Basics of XGBoost

XGBoost is an ensemble algorithm that belongs to the category of boosting algorithm in three typical methods of integration (bagging, boosting, and stacking). The main idea of this algorithm is to transform features to grow a tree and add trees constantly. In fact, each time a tree is added, a new function is learned to fit the residual of the last prediction. When the training is completed, k trees are obtained and subsequently the score of a sample can be predicted. According to the characteristics of the sample, a corresponding leaf node will be obtained in each tree, and each leaf node corresponds to a score that is finally added up to the corresponding score; therefore, the predicted value of the sample is obtained (Chen & Guestrin, 2016).

The objective function of the XGBoost algorithm comprises two parts, which can be defined as Eq. (1). The first part is used to measure the difference between the predicted and true scores, called the loss function. The other part is the regularization term, which is used to reduce the complexity of the objective function. Meanwhile, the regularization term comprises two parts, in which T represents the number of leaf nodes and w the score of the leaf node. The symbol γ is used to control the number of leaf nodes, and λ can be used to control the score of leaf nodes to be acceptable to prevent overfitting.

$$\text{Obj} = \sum_{i=1}^{n} l(y_i, \hat{y}_i) + \sum_{k=1}^{K} \Omega(f_k), \tag{1}$$

$$\Omega(f) = \gamma T + \frac{1}{2}\lambda \| w \|^2. \tag{2}$$

When t trees are generated, the newly generated tree is used to fit the residual of the last prediction. The predicted score can be written as Eq. (3). In addition, the objection function can be rewritten as Eq. (4).

$$\hat{y}_i^{(t)} = \hat{y}_i^{(t-1)} + f_t(x_i), \tag{3}$$

$$\text{Obj} = \sum_{i=1}^{n} l\left(y_i, \hat{y}_i^{(t-1)} + f_t(x_i)\right) + \Omega(f_t). \tag{4}$$

The next step is to obtain a suitable $f(t)$ that minimizes the target function. Taylor's second-order expansion at $f(t) = 0$ is used to approach the solution of XGBoost. The simplified objective function is approximated as follows:

$$\text{Obj}^{(t)} = \sum_{i=1}^{n} l\left(g_i f_t(x_i) + \frac{1}{2} h_i f_t^2(x_i)\right) + \Omega(f_t). \tag{5}$$

By transforming the formula above, the objective function can be written as a unary quadratic function on the leaf node score w; therefore, the optimal w_j^* and objective function values are solved. The score of each leaf node can be obtained using the derivation above.

$$w_j^* = -\frac{G_j}{H_j + \lambda}, \tag{6}$$

$$\text{Obj} = -\frac{1}{2} \sum_{j=1}^{T} \frac{G_j^2}{H_j + \lambda} + \gamma T. \tag{7}$$

The strategy of XGBoost is to utilize the objective function value above as the evaluation function to traverse all the feature points by a greedy algorithm. In particular, the split objective function value is compared with the gain of the objective function of a single leaf node under the predefined threshold that limits the tree growth significantly, and the split is performed only when the gain is greater than the threshold. Therefore, the best features and splitting points can be defined to determine the tree structure.

2.2 Three comparative supervised learning methods

2.2.1 ANN

The ANN model is a useful tool for geo-engineering applications owing to its high performance in the modeling of nonlinear multivariety problems (Zhang & Goh, 2013; Zhang & Goh, 2016). The multilayer perceptron (MLP) is an advanced version of the ANN, which was adapted in this study. It has been applied successfully to solve many difficult and diverse problems by training them with a highly popular learning algorithm, known as the back-propagation algorithm (Ocak & Seker, 2013). The MLP can be regarded as a directed graph comprising multiple node layers that are connected to the next layer individually. In addition to the input nodes, each node is a neuron with a nonlinear activation function.

Based on the biological neuron model, the basic structure of the MLP can be obtained. The typical MLP

includes input, output, or hidden layers, which are fully connected between different layers; this means that any neuron in the upper layer is connected to all neurons in the next layer. ANNs comprise three basic elements: activation function, weight, and bias. The activation function acts as a nonlinear map, which limits the output amplitude of the neuron to a certain range, generally limited to −1 to 1 or 0 to 1. The strength of the connection between neurons is represented by weight, and the magnitude of the weight indicates the likelihood size. The bias, which is an essential parameter in the model, is set to correctly classify the sample to ensure that the output value cannot be activated casually.

2.2.2 SVM

SVM is a novel type of learning algorithm based on statistical theory, which was pioneered by Boser, Guyon, and Vapnik (1992) and formally published in 1995 (Cortes & Vapnik, 1995). The SVM can be used to solve linear or nonlinear classification and regression problems (Samui, 2008a, 2008b; Ocak & Seker, 2013; Zhou, Li, & Mitri, 2015). In this section, the construction process of SVMs for regression problems is briefly introduced.

First, assuming a training sample $D = \{(x_1, y_1), (x_2, y_2), \cdots, (x_m, y_m)\}, y_i \in R$; the aim is to fit each point (x_i, y_i) of the training set to the linear model $y_i = w^T x + b$ as much as possible. The SVM is different from the traditional regression model, which can tolerate a maximum difference ϵ between the model output and the real value ($\epsilon > 0$); this means that the loss is calculated only when the absolute value of the difference between $f(x)$ and y is more than ϵ. Therefore, the loss function metric of the SVM regression model can be expressed as follows:

$$\text{Err}(x_i, y_i) = 0 \text{ for } |y_i - w^T x - b| \leq \epsilon,$$

$$\text{otherwise } \text{Err}(x_i, y_i) = |y_i - w^T x - b| - \epsilon,$$

where w is an adjustable weight vector, and b is the scalar threshold. Correspondingly, the SVM regression problem requires a small w, which can be formalized as follows:

$$\text{Minimize}: \frac{1}{2}\| w \|^2 + C \sum_{i=1}^{m} \ell_\epsilon(f(x_i) - y_i), \tag{8}$$

in which C is the regularization constant, and ℓ_ϵ is the ϵ-insensitive loss function. Using slack variables ξ_i and $\widehat{\xi}_i$, the formula above can be rewritten as follows:

$$\text{Minimize}: \frac{1}{2}\| w \|^2 + C \sum_{i=1}^{m} \left(\xi_i + \widehat{\xi}_i\right). \tag{9}$$

This optimization problem is solved using Lagrangian multipliers (Vapnik, 1998). For nonlinear regression problems, it is essential to map the input data into a high-dimensional feature space (Boser et al., 1992). To solve this

nodus, the kernel function $K(\boldsymbol{x}_i, \boldsymbol{x}_j) = \phi(\boldsymbol{x}_i)^{\mathrm{T}}\phi(\boldsymbol{x}_j)$ has been proposed to reduce the complexity of computation (Cortes & Vapnik, 1995); its solution is written as

$$f(\boldsymbol{x}) = \sum_{i=1}^{n}(a_i - a_i^*)K(\boldsymbol{x}_i \cdot \boldsymbol{x}_j) + b, \tag{10}$$

where a_i and a_i^* are Lagrangian multipliers; n is the number of support vectors (Gunn, 1998). In this case of SVM training, the kernel function that is a radial basis function was used. The kernel representation, which is a powerful alternative, uses linear machines for hypothesizing complex real-world problems.

2.2.3 MARS

MARS, proposed by Friedman (1991), is a statistical method for fitting the relationship between a set of input variables and dependent variables. Without assuming a latent correlation between the input and output, it is characterized with nonparametricity and is widely used in geotechinical engineering problems (Zhang, Goh, Zhang, Chen, & Xiao, 2015; Zhang, Zhang, & Goh, 2017; Goh, Zhang, Zhang, Zhang, & Xiao, 2017; Zhang, Zhang, Wang, et al., 2019). This method models the nonlinear responses between the variables of a system by a series of piecewise linear segments of differing gradients. The segments, i.e., each of the splines, are delimited by knots that indicate subdivisions between two data regions such that piecewise curves can be obtained. These piecewise curves are referred to as basis functions (BFs). MARS generates many BFs by searching in a stepwise manner. During this process, an adaptive regression algorithm is used for selecting the knot locations. MARS models are constructed in a two-phase procedure. The forward phase adds functions and finds potential knots to enhance the simulating performance, which results in an overfitting model. To mitigate this problem, the backward phase is used to prune the least effective terms. With these two construction phases, the MARS model can be constructed satisfactorily as a linear combination of BFs and their interactions and can be expressed as Eq. (11).

$$f(x) = \beta_0 + \sum_{n=1}^{N}\beta_n\lambda_n(x), \tag{11}$$

where each $\lambda_n(x)$ is a basis function. It can be a spline function, or the product of two or more spline functions already contained in the model. The coefficient β_n is a constant estimated using the least-squares method.

It is an adaptive technique because the selection of BFs and variable knot locations are data driven, which is specific to the problems to be solved. In addition, the functional relationship between the input variables and the output is not required, which allows for greater flexibility, bends, thresholds, and several types of BFs in modeling. An open-source code of MARS from Jekabsons (Jekabsons, 2010), which implements the main functionality of the MARS technique for the regression problem proposed in

(Friedman, 1991), was used to perform the analyses presented herein.

3 Case study

3.1 Brief description of ground conditions

Tunnel settlement data used were collected from three separate mass rapid transit projects of the North South and Circle Line in Singapore. The geographical location is shown in Fig. 1, with an enlarged portion to indicate the relative position of each construction line as well as the stations. Three of the different-colored points correspond to three construction lines' stations. The geological stratification of each construction site is shown in Fig. 2. It is obvious that the Dhoby Ghaut station to the Promenade station exhibits a complex geological condition, while other lines share the similar soil content. Four main formations covering the entire area of Singapore have been described in detail previously (Hulme & Burchell, 1999; Sharma, Chu, & Zhao, 1999; Izumi, Khatri, Norrish, & Davies, 2000; Shirlaw et al., 2003). For a brief introduction, one of the most widely distributed formations, i.e., the old alluvium, comprises dense alluvial silty sand and clay. As shown in Fig. 2(a), the Fort Canning boulder bed comprises a colluvial deposit of strong to very strong quartzite boulders in a hard, clayey silt matrix. In addition, the Jurong formation is primarily composed of residual soils, medium-plastic clayey silt, and sandy clay, as well as a limited volume of clayey to silty sand. The marine clay layer covers the entire research area, in which the formation is named the Kallang formation. In addition to the main content marine clay, which has an over consolidation tatio of approximately 1, the Kallang formation comprises layers of loose fluvial sand and moderately stiff fluvial clay.

According to survey data, soft soil is dominant in the construction of the projects, and the groundwater level is similar and stable among all construction sites; consequently, it is feasible to adopt the EPB shield technology. In addition, groundwater has not been pumped in all sites; therefore, it can be considered to be constant during the construction process, and the effect of groundwater table drawdown is negligible in the subsequent parameter input session.

3.2 Date collection and input parameters

The data for this study were obtained by installing ground settlement points at intervals of approximately 25 m along the tunnel alignment. A total of 148 monitoring points were used in all the projects. The representative parameters for each points were considered, which contained seven main characteristic variables and the final surface settlement value. The statistical characteristic values for each parameter are shown in Table 1.

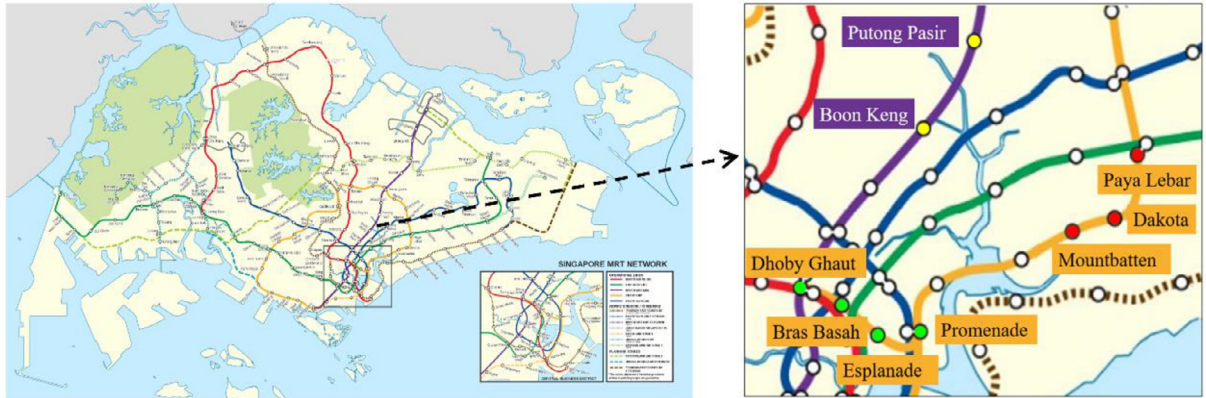These parameters consider three aspects of the parameters: geological conditions, tunnel geometry, and EPB
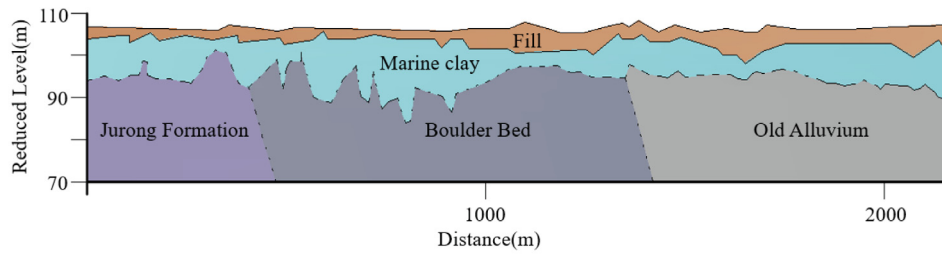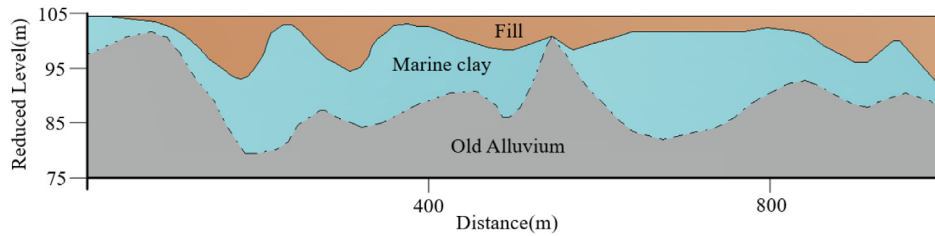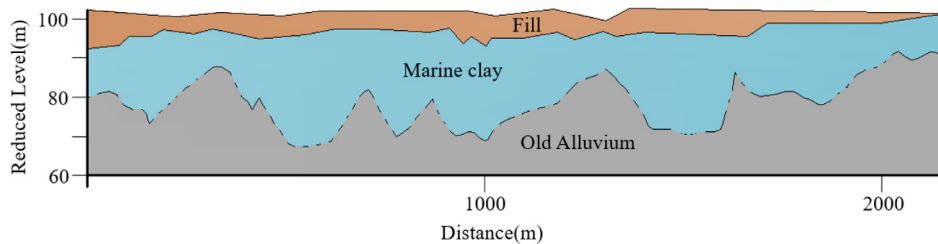
Fig. 1. Project locations in Singapore MRT Network.

(a) Dhoby Ghaut station to Promenade station

(b) Boon Keng station to Putong Pasir station

(c) Mountbatten station to Paya Lebar station

Fig. 2. Longitudinal profiles of the three projects (adapted from Goh et al., 2018).

operation factors. The geological conditions primarily involve the mean standard penetration test (SPT) value of the soil layers above the crown level up to the ground surface, S_1; average of the SPT values at the crown, middle, and invert levels, S_2; average moisture content of the soil layer driven through by the tunnel machine, C_M; and average elasticity modulus of the soil layer driven through by the tunnel machine, E.

Table 1
Statistical description of the model parameters (adapted from Goh et al., 2018).

Category	Symbol	Unit	Minimum	Maximum	Average	Standard deviation
Tunnel geometry	Cover H	m	8.5	30	17.5	4.3
EPB operation factors	Advance rate R_A	mm/min	9.5	52.1	30.8	10.9
	Earth pressure P_E	kPa	11	370	193.6	81.5
	Grout pressure P_G	kPa	27.7	700	258.6	154.9
Geological conditions	Mean moisture content C_M	%	5.95	66.48	27.1	18.7
	Mean soil elastic modulus E	MPa	5	120	72.9	50.8
	Mean SPT above crown level S_1	blows/300 mm	0.66	80.33	27.9	28.2
	Mean tunnel SPT S_2	blows/300 mm	0	100	57	41.8
Output	Surface settlement S_t	mm	0.2	98.5	13.6	17

For the tunnel geometry, the tunnel diameter and depth are major factors affecting ground deformation. However, as the internal diameter of all three projects tunnel was 5.8 m and the outside diameter was approximately 6.5 m, it was not considered as an input variable. The tunnel depth is changeable at different monitoring points, and the exposed stratum may change. Therefore, the tunnel cover depth H must be considered.

Moreover, because the EPB shield machine was used for tunneling in all projects, the operating factors will affect the change in surface settlement and the final settlement. The three primary parameters selected as inputs were the following: tunnel advance rate, R_A; EPB earth pressure, P_E; grout pressure used for injecting grout into the tail void, P_G.

Generally, a certain correlation exists between various parameters; a heat map of these seven parameters' correlation coefficient R is shown in Fig. 3. As shown, S_1, S_2, C_M, E, and P_G exhibit moderate correlations with the measured maximum surface settlement S_t, whereas the P_E is weakly correlated with S_t, while the R_A and H are almost independent of S_t. For the input parameters, it is clear that the C_M,

E, and S_2 are strongly correlated with each other, and the C_M is moderately correlated with P_G and S_1. Figure 3 illustrates the correlation of all parameters according to the R value (General guide: $|R| < 0.19$ means very weak correlation; $0.2 < |R| < 0.39$ means weak correlation; $0.4 < |R| < 0.59$ means moderate correlation; $0.6 < |R| < 0.79$ means strong correlation; $0.8 < |R| < 1$ means very strong correlation).

4 Results

4.1 Prediction performance of four models

To evaluate the predictive performance of the model accuracy, the k-fold cross-validation approach is frequently adopted on a database (Kohavi, 1995; Rodriguez, Perez, & Lozano, 2009; Wong, 2015). For k-fold cross-validation, data samples are randomly split into k equal subsamples, and a single subsample is used as validation data for testing the model, while the remaining $(k-1)$ subsamples are used as training data. This process is repeated k times such that each subset is used for validating once. Herein, the developed models are systematically compared with each other under a five-fold cross validation. The database was divided into two parts for all models, where approximately 80% (118 datasets) of the datasets were used as the training data and the remaining for testing purposes.

As shown in Fig. 4, all the data of the predicted $lg(S_t)$ against actual $lg(S_t)$ are scattered along the reference line. The left column of the scatter plots shows the accuracy of the training model of the machine learning methods, whereas the right represents the testing models' accuracy. It is clear that the accuracy of the training model is higher than that of testing model regardless of the k value. Most of the points of the XGBoost predictive model are closer to the line of equality, indicating a better prediction.

4.2 Comparison analyses and discussion

In this section, three evaluation indicators are introduced to quantitatively evaluate the accuracy of the training and testing models.
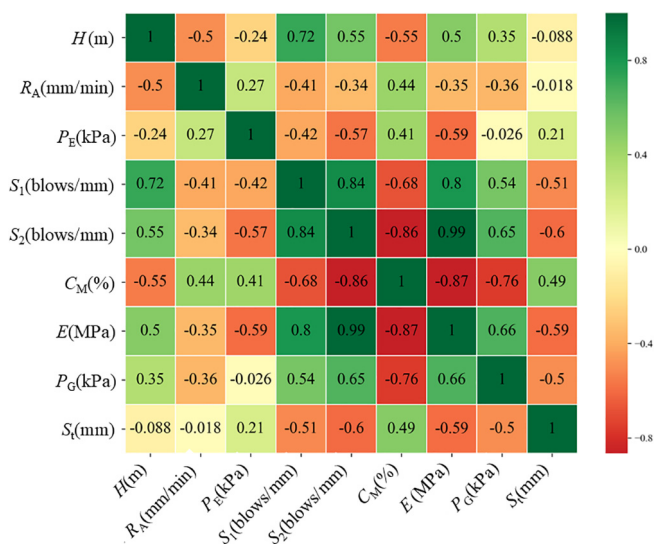

Fig. 3. Heat map of correlation coefficients.

The indices are root mean square error (RMSE), coefficient of determination (R^2), and bias factor b, expressed as Eqs. (12)–(14), respectively.

$$RMSE = \sqrt{\frac{1}{n} \sum_{i=1}^{n} (y_i - \hat{y}_i)^2}, \qquad (12)$$

$$R^2 = 1 - \frac{\sum (y_i - \hat{y}_i)^2}{\sum (y_i - \bar{y})^2}, \qquad (13)$$

$$b = \frac{1}{n} \sum_{i=1}^{n} \frac{y_i}{\hat{y}_i}, \qquad (14)$$

where y_i is the ith observed element, $\hat{y}_i$ is the ith predicted element, $\bar{y}_i$ is the mean of the observed values of y_i and n is the number of datasets used. Theoretically, the RMSE measures the deviation between the measured and predicted data, in which a lower RMSE value suggests a better performance. R^2 values that approach 1 indicates a better fit of the model to the data. Accordingly, a prediction model is considered excellent when the RMSE is 0 and $R^2 \approx 1$. The bias factor b is the sample mean of the actual value divided by the predicted value. The model prediction is unbiased when b is 1 (Ching & Phoon, 2014; D'Ignazio, Phoon, Tan, & Länsivaara, 2016).

The mean value (μ) and standard deviation (σ) of the evaluation index for the training and testing models

obtained with five-fold cross-validation ($k = 5$) are shown in Table 2. Furthermore, the values corresponding to different machine learning methods can be compared using every list, which enables an objective comparison between the models' performances. By comparing the RMSEs, the μ value of XGBoost is the minimum for both the training and testing sets. Similarly, the coefficient R^2 of XGBoost approaches 1, whereas those of the others are smaller. For the bias factor b, MARS performs better with a value approximately 1, indicating the unbiased property of this model. In general, the evaluation indices for XGBoost are slightly better than those of the other three algorithms, followed by the MARS model. The XGBoost-based model fits extremely well with the database in terms of accuracy and robustness. Moreover, the results indicate that the ensemble model XGBoost is superior to the single sophisticated algorithm for multisource data.

Feature importance selection, which calculates the contribution rate of each feature to the results, is critical for building an effective model. Different calculation methods can yield the corresponding feature importance after the prediction model is established. According to the prediction results, the XGBoost-based model exhibits the highest prediction accuracy. The importance of each feature based on the XGBoost method is shown in Fig. 5. The feature importance of the seven input parameters in this study is
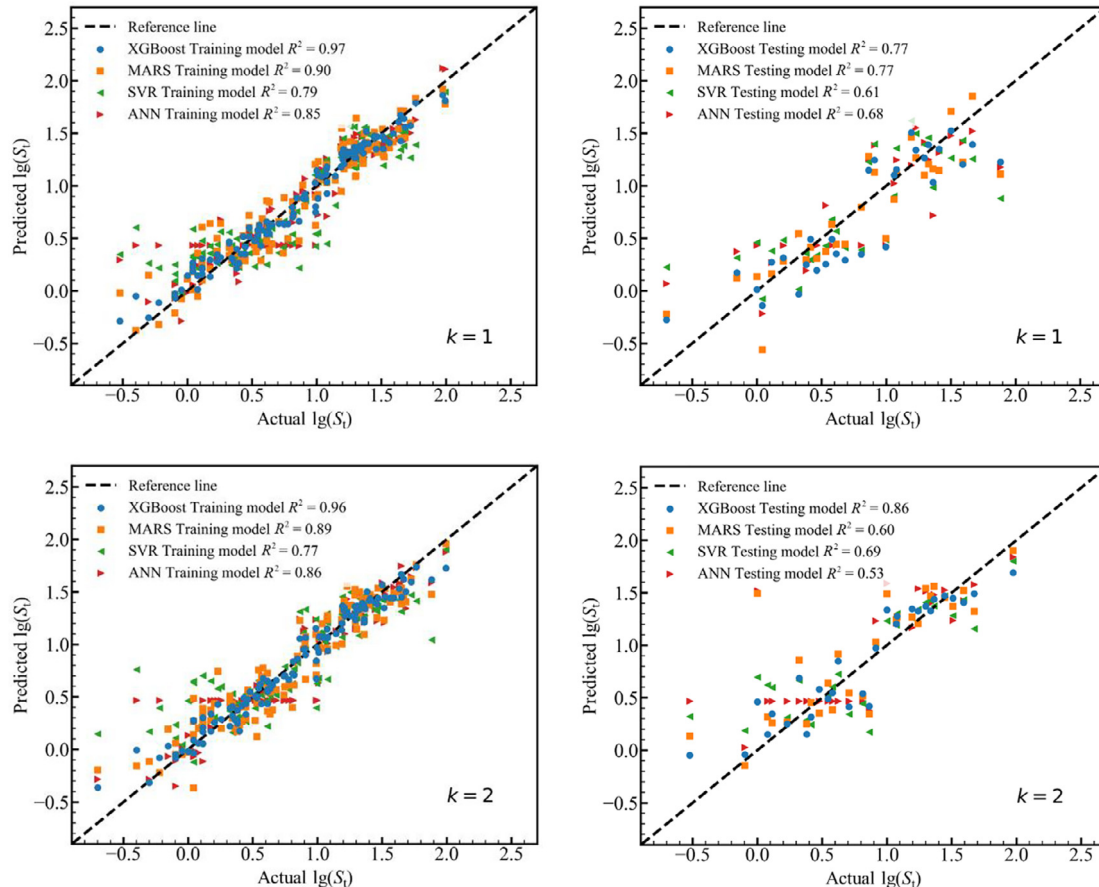

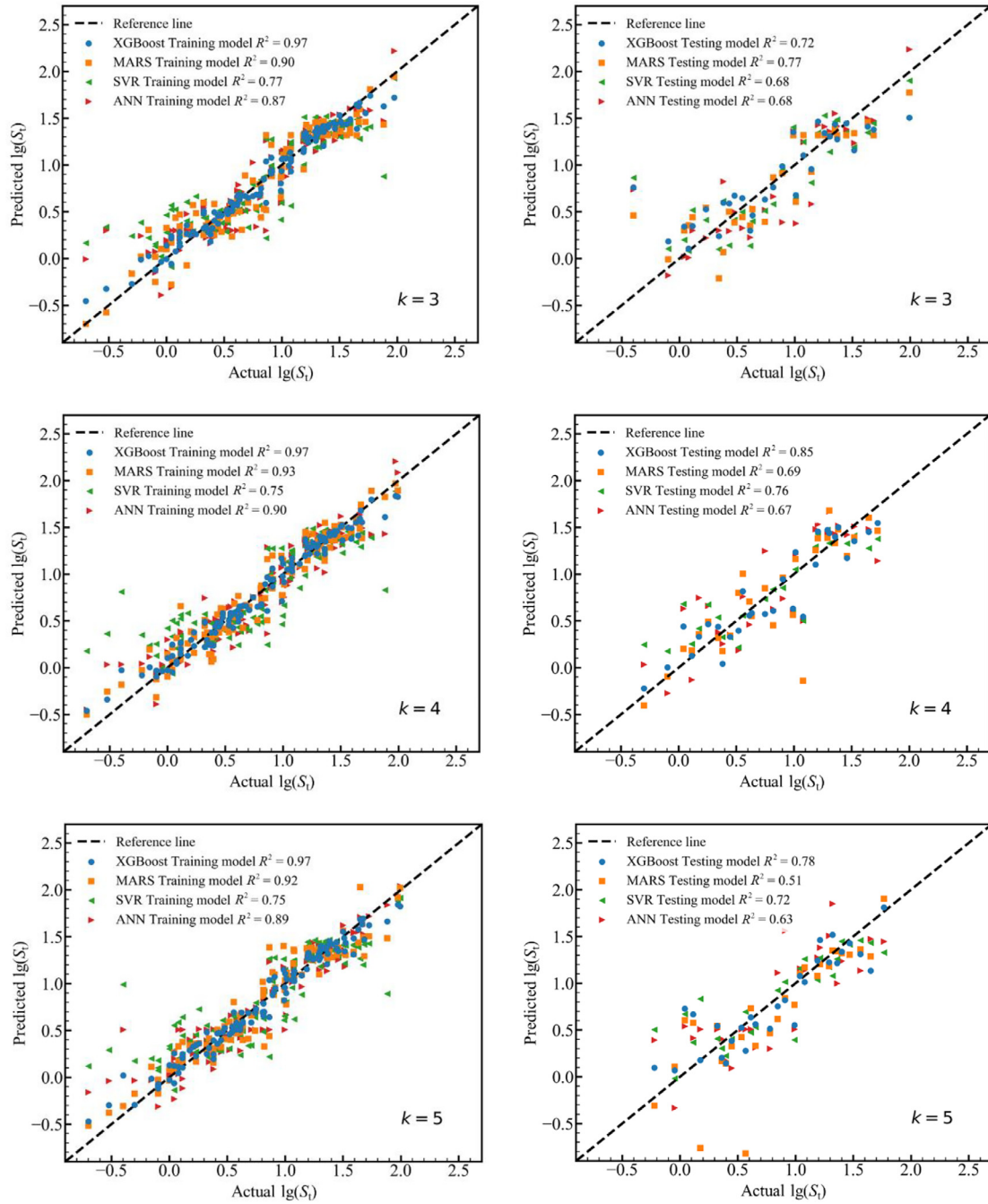Fig. 4. Predictive results under five-fold cross validation.

Fig 4. *(continued)*

Table 2
Comparison of models' performances.

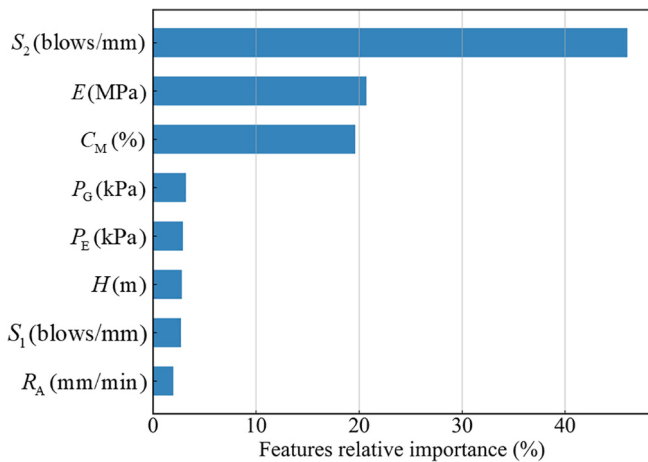| Evaluation index	RMSE				R^2				Bias			
	Training		Testing		Training		Testing		Training		Testing	
	μ	σ	μ	σ	μ	σ	μ	σ	μ	σ	μ	σ
XGBoost	0.11	0	0.26	0.03	0.97	0	0.79	0.05	1.09	0.23	0.81	0.4
MARS	0.17	0.01	0.32	0.04	0.91	0.01	0.67	0.09	1.04	0.13	0.97	0.2
SVM	0.28	0.01	0.32	0.03	0.77	0.01	0.69	0.05	0.92	0.07	1.14	0.22
ANN	0.23	0.01	0.31	0.04	0.84	0.02	0.71	0.06	1.37	0.32	1.11	0.35

Fig. 5. Feature importance of input variables.

represented numerically; a larger value indicates a better importance.

As shown in Fig. 5, the mean tunnel SPT (S_2) has the highest importance with 47%, followed by the mean soil elastic modulus (E) and mean moisture content (C_M); the other five variables only accounted for 3%. That is, the effect of geological conditions on tunnel excavation is obvious. Therefore, it is necessary to conduct a detailed investigation of the SPT value of the soil around the tunnel and the water content of the soil layer driven through by the tunnel machine. This result provides invaluable guidance for investigating the characteristics of tunnel excavation.

5 Summary and conclusions

An alternative method to predict surface settlement caused by tunneling using XGBoost, ANN, SVM, and MARS algorithms based on five-fold cross-validation was presented herein. Databases from three separate mass rapid transit projects of the Circle Line in Singapore were compiled.

The data points of the XGBoost predictive model were closer to the line of equality for the training set; it exhibited the highest accuracy, whereas MARS a slightly lower accuracy. To evaluate the model more accurately and quantitatively, the RMSE, R^2, and b were presented to analyze the predictive results of soft computing models. By comparing the μ and σ of those three indices, it was observed that the XGBoost algorithm exhibited excellent performance and that this ensemble method was superior to the single algorithm for multisource data. Nevertheless, the interpretability of the XGBoost-based model was lower than those of the other three models. In general, these four models are suitable for determining EPB tunneling projects in similar geological conditions.

In addition, the relative importance of the input variables was presented based on the XGBoost algorithm, in which the S_2 exhibited the highest importance followed by the E and C_M. This result differed from the importance of the features presented by Goh et al. (2018). This was because the database was divided into different parts for both studies. Additionally, the value range was limited. These aspects may change the relative importance of the features. It is noteworthy that the data and features determine the upper limit of accuracies by soft computing methods, while the various models and algorithms approach this limit differently. Hence, high-quality datasets and well-extracted features that are closely related with the dependent responses are critical for the successful application of soft computing methods.

Acknowledgement

Declaration of Competing Interest

The authors wish to confirm that there are no known conflicts of interests associated with this publication and there has been no significant financial support for this work that could have influenced its outcome.

References

Adoko, A. C., Jiao, Y. Y., Wu, L., Wang, H., & Wang, Z. H. (2013). Predicting tunnel convergence using multivariate adaptive regression spline and artificial neural network. *Tunnelling and Underground Space Technology, 38*, 368–376.

Adoko, A. C., Zuo, Q. J., & Wu, L. (2011). A fuzzy model for high-speed railway tunnel convergence prediction in weak rock. *Electronic Journal of Geotechnical Engineering, 16*(1), 275–281.

Ahangari, K., Moeinossadat, S. R., & Behnia, D. (2015). Estimation of tunnelling-induced settlement by modern intelligent methods. *Soils and Foundations, 55*(4), 737–748.

Bilgin, N., Ozbayir, T., Sozak, N., & Eyigun, Y. (2009). Factors affecting the economy and the efficiency of metro tunnel drivage with two TBM's in Istanbul in very fractured rock. In ITA-World Tunnel Congress.

Boser, B. E., Guyon, I. M., & Vapnik, V. N. (1992). A training algorithm for optimal margin classifiers. In *Proceedings of the fifth annual workshop on Computational learning theory*. Pittsburgh, Pennsylvania, USA. New York, USA: ACM Press (pp. 144–152).

Bouayad, D., Emeriault, F., & Maza, M. (2015). Assessment of ground surface displacements induced by an earth pressure balance shield tunneling using partial least squares regression. *Environmental Earth Sciences, 73*(11), 7603–7616.

Chakeri, H., Hasanpour, R., Hindistan, M. A., & Ünver, B. (2011). Analysis of interaction between tunnels in soft ground by 3D numerical modeling. *Bulletin of Engineering Geology and the Environment, 70*(3), 439–448.

Chapman, D. N., Ahn, S. K., & Hunt, D. V. (2007). Investigating ground movements caused by the construction of multiple tunnels in soft ground using laboratory model tests. *Canadian Geotechnical Journal, 44*(6), 631–643.

Chen, F. Y., Wang, L., & Zhang, W. G. (2019). Reliability assessment on stability of tunneling perpendicularly beneath an existing tunnel considering spatial variabilities of rock mass properties. *Tunnelling and Underground Space Technology, 88*, 276–289.

Chen, T., & Guestrin, C. (2016). Xgboost: A scalable tree boosting system. In *Proceedings of the 22nd acm sigkdd international conference on knowledge discovery and data mining* (pp. 785–794). ACM.

Cheng, M. Y., Tsai, H. C., Ko, C. H., & Chang, W. T. (2008). Evolutionary fuzzy neural inference system for decision making in geotechnical engineering. *Journal of Computing in Civil Engineering, 22*(4), 272–280.

Ching, J., & Phoon, K. K. (2014). Transformations and correlations among some clay parameters—The global database. *Canadian Geotechnical Journal, 51*(6), 663–685.

Chou, W. I., & Bobet, A. (2002). Predictions of ground deformations in shallow tunnels in clay. *Tunnelling and Underground Space Technology, 17*(1), 3–19.

Cortes, C., & Vapnik, V. (1995). Support-vector networks. *Machine Learning, 20*(3), 273–297.

D'Ignazio, M., Phoon, K. K., Tan, S. A., & Länsivaara, T. T. (2016). Correlations for undrained shear strength of Finnish soft clays. *Canadian Geotechnical Journal, 53*(10), 1628–1645.

Ding, Z., Wei, X. J., & Wei, G. (2017). Prediction methods on tunnel-excavation induced surface settlement around adjacent building. *Geomechanics and Engineering, 12*(2), 185–195.

Ercelebi, S. G., Copur, H., & Ocak, I. (2011). Surface settlement predictions for Istanbul Metro tunnels excavated by EPB-TBM. *Environmental Earth Sciences, 62*(2), 357–365.

Fang, Y., Chen, Z., Tao, L., Cui, J., & Yan, Q. (2019). Model tests on longitudinal surface settlement caused by shield tunnelling in sandy soil. *Sustainable Cities and Society, 47*, 101504.

Friedman, J. H. (1991). Multivariate adaptive regression splines. *The Annals of Statistics, 19*(1), 1–67.

Goh, A. T. C., Zhang, W., Zhang, Y., Xiao, Y., & Xiang, Y. (2018). Determination of earth pressure balance tunnel-related maximum surface settlement: A multivariate adaptive regression splines approach. *Bulletin of Engineering Geology and the Environment, 77*(2), 489–500.

Goh, A. T. C., Zhang, Y. M., Zhang, R. H., Zhang, W. G., & Xiao, Y. (2017). Evaluating stability of underground entry-type excavations using multivariate adaptive regression splines and logistic regression. *Tunnelling and Underground Space Technology, 70*, 148–154.

Gong, W., Luo, Z., Juang, C. H., Huang, H., Zhang, J., & Wang, L. (2014). Optimization of site exploration program for improved prediction of tunneling-induced ground settlement in clays. *Computers and Geotechnics, 56*, 69–79.

Gunn, S. R. (1998). Support vector machines for classification and regression. *ISIS technical report, 14*(1), 5–16.

Huang, H., Gong, W., Khoshnevisan, S., Juang, C. H., Zhang, D., & Wang, L. (2015). Simplified procedure for finite element analysis of the longitudinal performance of shield tunnels considering spatial soil variability in longitudinal direction. *Computers and Geotechnics, 64*, 132–145.

Huang, Q., Huang, H., Ye, B., Zhang, D., & Zhang, F. (2018). Evaluation of train-induced settlement for metro tunnel in saturated clay based on an elastoplastic constitutive model. *Underground Space, 3*(2), 109–124.

Hulme, T. W., & Burchell, A. J. (1999). Tunnelling projects in Singapore: An overview. *Tunnelling and Underground Space Technology, 14*(4), 409–418.

Izumi, C., Khatri, N. N., Norrish, A., & Davies, R. (2000). Stability and settlement due to bored tunneling for LTA, NEL. In *Proceedings of International conference on tunnels and underground structures*, Singapore (pp. 555–560).

Jekabsons, G. (2010). *VariReg: A software tool for regression modeling using various modeling methods*. Riga: Technical University.

Kim, C. Y., Bae, G. J., Hong, S. W., Park, C. H., Moon, H. K., & Shin, H. S. (2001). Neural network based prediction of ground surface settlements due to tunnelling. *Computers and Geotechnics, 28*(6/7), 517–547.

Kohavi, R. (1995). A study of cross-validation and bootstrap for accuracy estimation and model selection. In *Proceedings of the Fourteenth International Joint Conference on Artificial Intelligence (IJCAI)*, Montreal, Quebec, Canada, vol. 14, No.2, pp. 1137–1145.

Kohestani, V. R., & Bazarganlari, M. R. (2017). Prediction of maximum surface settlement caused by earth pressure balance shield tunneling using random forest. *Journal of AI and Data Mining, 5*(1), 127–135.

Lambrughi, A., Rodríguez, L. M., & Castellanza, R. (2012). Development and validation of a 3D numerical model for TBM–EPB mechanised excavations. *Computers and Geotechnics, 40*, 97–113.

Lessmann, S., Baesens, B., Seow, H. V., & Thomas, L. C. (2015). Benchmarking state-of-the-art classification algorithms for credit scoring: An update of research. *European Journal of Operational Research, 247*(1), 124–136.

Loganathan, N., & Poulos, H. G. (1998). Analytical prediction for tunneling-induced ground movements in clays. *Journal of Geotechnical and Geoenvironmental Engineering, 124*(9), 846–856.

Lu, H., Shi, J., Wang, Y., & Wang, R. (2019). Centrifuge modeling of tunneling-induced ground surface settlement in sand. *Underground Space, 4*(4), 302–309.

Mahdevari, S., & Torabi, S. R. (2012). Prediction of tunnel convergence using artificial neural networks. *Tunnelling and Underground Space Technology, 28*, 218–228.

Mahdevari, S., Torabi, S. R., & Monjezi, M. (2012). Application of artificial intelligence algorithms in predicting tunnel convergence to avoid TBM jamming phenomenon. *International Journal of Rock Mechanics and Mining Sciences, 55*, 33–44.

Mair, R. J., Taylor, R. N., & Bracegirdle, A. (1993). Subsurface settlement profiles above tunnels in clays. *Geotechnique, 43*(2), 315–320.

Marshall, A. M., Farrell, R. P., Klar, A., & Mair, R. (2012). Tunnels in sands: The effect of size, depth and volume loss on greenfield displacements. *Géotechnique, 62*(5), 385–399.

Mroueh, H., & Shahrour, I. (2002). Three-dimensional finite element analysis of the interaction between tunneling and pile foundations. *International Journal for Numerical and Analytical Methods in Geomechanics, 26*(3), 217–230.

Nanni, L., & Lumini, A. (2009). An experimental comparison of ensemble of classifiers for bankruptcy prediction and credit scoring. *Expert Systems With Applications, 36*(2), 3028–3033.

Neaupane, K. M., & Adhikari, N. R. (2006). Prediction of tunneling-induced ground movement with the multi-layer perceptron. *Tunnelling and Underground Space Technology, 21*(2), 151–159.

Ng, C. W., & Lee, G. T. (2005). Three-dimensional ground settlements and stress-transfer mechanisms due to open-face tunnelling. *Canadian Geotechnical Journal, 42*(4), 1015–1029.

Ocak, I. (2009). Environmental effects of tunnel excavation in soft and shallow ground with EPBM: The case of Istanbul. *Environmental Earth Sciences, 59*(2), 347–352.

Ocak, I., & Seker, S. E. (2013). Calculation of surface settlements caused by EPBM tunneling using artificial neural network, SVM, and Gaussian processes. *Environmental Earth Sciences, 70*(3), 1263–1276.

Park, K. H. (2005). Analytical solution for tunnelling-induced ground movement in clays. *Tunnelling and Underground Space Technology, 20*(3), 249–261.

Rodriguez, J. D., Perez, A., & Lozano, J. A. (2009). Sensitivity analysis of k-fold cross validation in prediction error estimation. *IEEE Transactions on Pattern Analysis And Machine Intelligence, 32*(3), 569–575.

Samui, P. (2008a). Prediction of friction capacity of driven piles in clay using the support vector machine. *Canadian Geotechnical Journal, 45*(2), 288–295.

Samui, P. (2008b). Support vector machine applied to settlement of shallow foundations on cohesionless soils. *Computers and Geotechnics, 35*(3), 419–427.

Santos, O. J., Jr, & Celestino, T. B. (2008). Artificial neural networks analysis of São Paulo subway tunnel settlement data. *Tunnelling and Underground Space Technology, 23*(5), 481–491.

Sharma, J. S., Chu, J., & Zhao, J. (1999). Geological and geotechnical features of Singapore: An overview. *Tunnelling and Underground Space Technology, 14*(4), 419–431.

Shirlaw, J. N., Ong, J. C. W., Rosser, H. B., Tan, C. G., Osborne, N. H., & Heslop, P. E. (2003). Local settlements and sinkholes due to EPB tunnelling. In *Proceedings of the Institution of Civil Engineers-Geotechnical Engineering*, 156(4), 193–211.

Suwansawat, S., & Einstein, H. H. (2006). Artificial neural networks for predicting the maximum surface settlement caused by EPB shield tunneling. *Tunnelling and Underground Space Technology, 21*(2), 133–150.

Verruijt, A., & Booker, J. R. (1996). Surface settlements due to deformation of a tunnel in an elastic half place. *Géotechnique, 46*(4), 753–756.

Wang, D. D., Qiu, G. Q., Xie, W. B., & Wang, Y. (2012). Deformation prediction model of surrounding rock based on GA-LSSVM-Markov. *Natural Science, 4*(2), 85–90.

Wong, T. T. (2015). Performance evaluation of classification algorithms by k-fold and leave-one-out cross validation. *Pattern Recognition, 48*(9), 2839–2846.

Xiang, Y. Z., Liu, H. L., Zhang, W. G., Chu, J., Zhou, D., & Xiao, Y. (2018). Application of transparent soil model test and DEM simulation in study of tunnel failure mechanism. *Tunnelling and Underground Space Technology, 74*, 178–184.

Xie, X., Wang, Q., Huang, Z., & Qi, Y. (2018). Parametric analysis of mixshield tunnelling in mixed ground containing mudstone and protection of adjacent buildings: Case study in Nanning metro. *European Journal of Environmental and Civil Engineering, 22*(sup1), s130–s148.

Xu, J., & Xu, Y. (2011). Grey correlation-hierarchical analysis for metro-caused settlement. *Environmental Earth Sciences, 64*(5), 1249–1256.

Yao, B. Z., Yang, C. Y., Yao, J. B., & Sun, J. (2010). Tunnel surrounding rock displacement prediction using support vector machine. *International Journal of Computational Intelligence Systems, 3*(6), 843–852.

Zhang, W. G., & Goh, A. T. C. (2013). Multivariate adaptive regression splines for analysis of geotechnical engineering systems. *Computers and Geotechnics, 48*, 82–95.

Zhang, W. G., & Goh, A. T. C. (2016). Multivariate adaptive regression splines and neural network models for prediction of pile drivability. *Geoscience Frontiers, 7*(1), 45–52.

Zhang, W. G., Goh, A. T. C., Zhang, Y. M., Chen, Y. M., & Xiao, Y. (2015). Assessment of soil liquefaction based on capacity energy concept and multivariate adaptive regression splines. *Engineering Geology, 188*, 29–37.

Zhang, W. G., Wu, C. Z., Li, Y. Q., Wang, L., & Samui, P. (2021). Assessment of pile drivability using random forest regression and multivariate adaptive regression splines. Georisk: Assessment and Management of Risk for Engineered Systems and Geohazards, *15*(1), 27–40.

Zhang, W. G., Zhang, R. H., Wang, W., Zhang, F., & Goh, A. T. C. (2019). A Multivariate Adaptive Regression Splines model for determining horizontal wall deflection envelope for braced excavations in clays. *Tunnelling and Underground Space Technology, 84*, 461–471.

Zhang, W. G., Zhang, R. H., Wu, C. Z., Goh, A. T. C., Lacasse, S., Liu, Z. Q., & Liu, H. L. (2020). State-of-the-art review of soft computing applications in underground excavations. *Geoscience Frontiers, 11*(4), 1095–1106.

Zhang, W. G., Zhang, Y. M., & Goh, A. T. C. (2017). Multivariate adaptive regression splines for inverse analysis of soil and wall properties in braced excavation. *Tunnelling and Underground Space Technology, 64*, 24–33.

Zhou, J., Li, X., & Mitri, H. S. (2015). Comparative performance of six supervised learning methods for the development of models of hard rock pillar stability prediction. *Natural Hazards, 79*(1), 291–316.